MITC9 Shell elements based on RMVT and CUF for the analysis of laminated composite plates and shells

MITC9 SHELL ELEMENTS BASED ON RMVT AND CUF FOR THE ANALYSIS OF LAMINATED COMPOSITE PLATES AND SHELLS

Maria Cinefra[1], S. Keshava Kumar[2], Erasmo Carrera[1,3]

[1]Department of Mechanical and Aerospace Engineering, Politecnico di Torino, Italy
E-mail: maria.cinefra@polito.it

[2]Department of Aerospace Engineering, Defence Institute of Advanced Technology, Pune, India
E-mail: keshava.srao@gmail.com

[3]Laboratory of Intelligent Materials and Structures Tambov State Technical University, Russia
E-mail: erasmo.carrera@polito.it

Abstract

In this paper, we present some advanced shell models for the analysis of orthotropic multilayered structures in which the mechanical and physical properties may change in the thickness direction. The finite element method showed successful performances to approximate the solutions of the advanced structures. In this regard, two variational formulations are available to reach the stiffness matrices, the principle of virtual displacement (PVD) and the Reissner mixed variational theorem (RMVT). Here we introduce a strategy similar to MITC (Mixed Interpolated of Tensorial Components) approach, in the RMVT formulation, in order to construct an advanced locking-free finite element. Moreover, assuming the transverse stresses as independent variables, the continuity at the interfaces between layers is easily imposed. We show that in the RMVT context, the element exhibits both properties of convergence and robustness when comparing the numerical results with benchmark solutions from literature, even for higher span to thickness ratios, and both interlayer continuity conditions and boundary conditions are fully satisfied.

1. Introduction

Multilayered composite structures are used in many fields, and their usage is increasing day by day. Examples of multilayered structures are sandwich constructions, composite structures made of orthotropic laminae or layered structures made of different isotropic layers (such as those employed for thermal protection). In most of the applications, these structures mostly appear as flat (plates) or curved panels (shells).

The analysis of multilayered structures is difficult with respect to the analysis of homogenous (homogeneity of the structure predominantly in the thickness direction) plates and shells. A number of interesting and complicating effects arise when their mechanical behaviour as well as failure mechanisms have to be coherently understood. This is due to the intrinsic discontinuity of the mechanical properties at each layer–interface, this discontinuity leads to development of high interfacial shear stresses. An accurate description of the stress and strain fields of these structures requires theories that are able to satisfy the so–called Interlaminar Continuity (IC) conditions for the transverse stresses (see Whitney [1], and Pagano [2], as examples). Transverse anisotropy of multilayered structures depending on the number of layers and their orientation makes it difficult to find closed form solutions, and this leads to the use of approximated solutions techniques. It can therefore be concluded that the use of both refined two–dimensional theories and computational methods become mandatory to solve practical problems related to multilayered structures, to obtain the solution in first place and to obtain best approximations of stresses.

Among the several computational methods available in literature, the Finite Element Method (FEM) has played and continues to play a significant role. In this work, as an extension of the previous work [3] by the first and third authors of this article, the Reissner's Mixed Variational Theorem (RMVT) is used to derive a set of algebraic equations through Lagrangian finite elements for orthotropic laminated composite structures. As a main property, RMVT permits one to assume two independent fields for displacement and transverse stress variables. The resulting advanced finite elements therefore describe *a priori* interlaminar continuous transverse stress fields.

For a complete and rigorous understanding of the foundations of RMVT, reference can be made to the articles by Professor Reissner [4–6] and the review article by Carrera [7]. The first application of RMVT to modelling of multilayered flat structures was performed by Murakami [8, 9]. He introduced a first order displacement field in his papers, in conjunction with an independent parabolic transverse stress layer-wise (LW) field in each layer

(transverse normal stress and strain were discarded). An extension to a higher order displacement field was adopted by Toledano and Murakami in [10]. While in [11], they extended the RMVT to a layer-wise description of both displacement and transverse stress fields. These papers [8–11] should be considered as the fundamental works in the applications of RMVT as a tool to model multilayered structures. Further discussions on RMVT were provided by Soldatos [12]. A generalization, proposing a systematic use of RMVT as a tool to furnish a class of two dimensional theories for multilayered plate analysis, was presented by Carrera [13, 14]. The order of displacement fields in the layer was taken as a free parameter of the theories. Applications of what is reported in [13, 14] have been given in several other papers [15–22], in which closed-form solutions are considered. Layer-wise mixed analyses were performed in [23] for the static case. As a fundamental result, the numerical analysis demonstrated that RMVT furnishes a quasi three-dimensional a-priori description of transverse stresses, including transverse normal components. Sandwich plates were also considered in [16]. Recently, Messina [24] has compared RMVT results to PVD (Principle of Virtual Displacements) ones. Transverse normal stresses were, however, discarded in this work. In [25–27], Carrera and Demasi developed multilayered plate elements based on RMVT, that were able to give a quasi–three-dimensional description of stress/strain fields. But in these works, they still employ the selective reduced integration [28] to overcome the locking phenomenon.

Recently, authors adopted the Mixed Interpolation of Tensorial Components (MITC) to contrast the locking. According to this technique, the strain components are not directly computed from the displacements but they are interpolated within each element using a specific interpolation strategy for each component. For more details about MITC, the readers can refer to the works [29–33]. In [34] and [35], the authors formulated plate/shell elements based on displacement formulation that showed good properties of convergence thanks to the use of the MITC. In [3] authors formulated plate/shell elements based on RMVT with the use of MITC method to elevate shear locking phenomenon and showed the performance of shell element for isotropic sandwich structures. The idea of this work is to interpolate the transverse stresses (that are modelled a-priori by the RMVT) using the same strategy of the MITC. In this way, the RMVT permits both to satisfy IC conditions and to withstand the locking phenomenon, and implement it for laminated composite structures, with each lamina having orthotropic lamina properties.

The shell elements here proposed have nine nodes. The displacement field and transverse fields are defined according to the Unified Formulation [36] introduced by Carrera. In particular, higher-order layer-wise models are used for the analysis of multilayered structures. The shear stresses σ_{xz} and σ_{yz} are interpolated in each element according to the MITC in order to contrast the shear locking. Also the in-plane strains are re-interpolated in order to withstand the membrane locking. Comparisons with 3D solutions are provided and they demonstrate the efficiency of elements presented. The results obtained using PVD and RMVT are compared with 3D solutions. In particular, RMVT transverse shear stresses obtained using a-priori field variables are compared with a-posteriori shear stresses obtained from PVD. The effect of not performing MITC corrections on shear stresses and its effects on thin shells and plates is detailed out. The article comprehensively lists the results for plates and shells obtained using most of the theories available in Carrera Unified Formulation.

2. Reissner's Mixed Variational Theorem

By considering a doubly-curved shell with constant radii of curvature and naming the curvilinear reference system as (α, β, z), the stress vector $\boldsymbol{\sigma} = (\sigma_i), \quad i = 1, ...6$ can be written in terms of the in-plane and transverse components as $\boldsymbol{\sigma} = [\boldsymbol{\sigma}_p \;\; \boldsymbol{\sigma}_n]$ with:

$$\boldsymbol{\sigma}_p = [\sigma_{\alpha\alpha} \; \sigma_{\beta\beta} \; \sigma_{\alpha\beta}]^T, \quad \boldsymbol{\sigma}_n = [\sigma_{\alpha z} \; \sigma_{\beta z} \; \sigma_{zz}]^T \tag{1}$$

and analogously the strain vector $\boldsymbol{\epsilon} = (\epsilon_i)$, $i = 1, ...6$ can be written in terms of the in-plane and transverse components as $\boldsymbol{\epsilon} = [\boldsymbol{\epsilon}_p \; \boldsymbol{\epsilon}_n]$, with:

$$\boldsymbol{\epsilon}_p = [\epsilon_{\alpha\alpha} \; \epsilon_{\beta\beta} \; \epsilon_{\alpha\beta}]^T, \quad \boldsymbol{\epsilon}_n = [\epsilon_{\alpha z} \; \epsilon_{\beta z} \; \epsilon_{zz}]^T \tag{2}$$

The PVD variational equation is written as:

$$\int_{\Omega_k}\int_{A_k} \left(\delta {\boldsymbol{\epsilon}^k_{pG}}^T \boldsymbol{\sigma}^k_{pH} + \delta {\boldsymbol{\epsilon}^k_{nG}}^T \boldsymbol{\sigma}^k_{nH} \right) H^k_\alpha H^k_\beta \, d\Omega_k dz = \int_{\Omega_k}\int_{A_k} \delta \mathbf{u}^k \mathbf{p}^k H^k_\alpha H^k_\beta d\Omega_k dz \tag{3}$$

where Ω_k and A_k are the integration domains in the plane and in the thickness direction, respectively. The member on the left hand side of the equation represents the variation of the internal work, while the member on the right hand side of the equation represents the external work done due to applied loads. Also, $\mathbf{u}^k = [u^k_\alpha \; u^k_\beta \; u^k_z]^T$ is

the vector of displacements and $\boldsymbol{p}^k = \{p^k_\alpha(\alpha,\beta,z), p^k_\beta(\alpha,\beta,z), p^k_z(\alpha,\beta,z)\}$ is the mechanical load applied to the structure at layer level.

The subscript H means that the stresses are computed by Hooke's law, while the subscript G means that the strains are computed from geometrical relations. The superscript T stands for transposition operation, V represents the 3D multilayered body volume. The metric coefficients are represented by H_α and H_β and they have the following explicit form, where R_α and R_β are the principal radii of curvature along the coordinates α and β, respectively:

$$H_\alpha = (1 + z/R_\alpha)\,, \quad H_\beta = (1 + z/R_\beta). \tag{4}$$

In the RMVT formulation the transverse stresses are assumed as independent variables and denoted by $\boldsymbol{\sigma}_{nM}$ (M stands for *Model*). The transverse strains are evaluated by Hooke's law and denoted by $\boldsymbol{\epsilon}_{nH}$. They should be related to the geometrical strains $\boldsymbol{\epsilon}_{nG}$ by the constraint equation:

$$\boldsymbol{\epsilon}_{nH} = \boldsymbol{\epsilon}_{nG}. \tag{5}$$

By adding in (3) the compatibility condition (5) through a Lagrange multipliers field, which turn out to be transverse stresses, one then obtain the RMVT formulation:

$$\begin{aligned} &\int_{\Omega_k}\int_{A_k} \left[\delta\boldsymbol{\epsilon}^T_{pG}\boldsymbol{\sigma}_{pH} + \delta\boldsymbol{\epsilon}^T_{nG}\boldsymbol{\sigma}_{nM} + \delta\boldsymbol{\sigma}^T_{nM}(\boldsymbol{\epsilon}_{nG} - \boldsymbol{\epsilon}_{nH})\right] H^k_\alpha H^k_\beta \, d\Omega_k dz \\ &\qquad = \int_{\Omega_k}\int_{A_k} \delta\boldsymbol{u}^k \boldsymbol{p}^k H^k_\alpha H^k_\beta d\Omega_k dz \end{aligned} \tag{6}$$

The third 'mixed' term on the left hand side, variationally enforces the compatibility of the transverse strain components.

3. The constitutive equations and the geometrical relations

In this section we will explain in detail the construction of RMVT employing the Hooke's law and the geometrical relations (see for example [26],[27]).

Referring to the Hooke's law for orthotropic material $\sigma_i = \tilde{C}_{ij}\epsilon_j,\ i,j = 1,...6$ the constitutive equations become:

$$\begin{aligned} \boldsymbol{\sigma}_{pH} &= \tilde{\mathbf{C}}_{pp}\boldsymbol{\epsilon}_{pG} + \tilde{\mathbf{C}}_{pn}\boldsymbol{\epsilon}_{nG} \\ \boldsymbol{\sigma}_{nH} &= \tilde{\mathbf{C}}_{np}\boldsymbol{\epsilon}_{pG} + \tilde{\mathbf{C}}_{nn}\boldsymbol{\epsilon}_{nG} \end{aligned} \tag{7}$$

where the material matrices are:

$$\begin{aligned} &\tilde{\mathbf{C}}_{pp} = \begin{bmatrix} \tilde{C}_{11} & \tilde{C}_{12} & \tilde{C}_{16} \\ \tilde{C}_{12} & \tilde{C}_{22} & \tilde{C}_{26} \\ \tilde{C}_{16} & \tilde{C}_{26} & \tilde{C}_{66} \end{bmatrix} \quad \tilde{\mathbf{C}}_{pn} = \begin{bmatrix} 0 & 0 & \tilde{C}_{13} \\ 0 & 0 & \tilde{C}_{23} \\ 0 & 0 & \tilde{C}_{36} \end{bmatrix} \\ &\tilde{\mathbf{C}}_{np} = \tilde{\mathbf{C}}^T_{pn}; \quad \tilde{\mathbf{C}}_{nn} = \begin{bmatrix} \tilde{C}_{55} & \tilde{C}_{45} & 0 \\ \tilde{C}_{45} & \tilde{C}_{44} & 0 \\ 0 & 0 & \tilde{C}_{33} \end{bmatrix} \end{aligned} \tag{8}$$

From the second equation of (7) we obtain

$$\boldsymbol{\epsilon}_{nH} = -(\tilde{\mathbf{C}}_{nn})^{-1}\tilde{\mathbf{C}}_{np}\boldsymbol{\epsilon}_{pG} + (\tilde{\mathbf{C}}_{nn})^{-1}\boldsymbol{\sigma}_{nM} \tag{9}$$

We note that the right side of the above relation can be assumed as definition of transverse strains from Hooke's law, $\boldsymbol{\epsilon}_{nH}$. After substitution into the first equation of (7) we obtain:

$$\boldsymbol{\sigma}_{pH} = [\tilde{\mathbf{C}}_{pp} - \tilde{\mathbf{C}}_{pn}(\tilde{\mathbf{C}}_{nn})^{-1}\tilde{\mathbf{C}}_{np}]\boldsymbol{\epsilon}_{pG} \ + \tilde{\mathbf{C}}_{pn}(\tilde{\mathbf{C}}_{nn})^{-1}\boldsymbol{\sigma}_{nM}. \tag{10}$$

The transverse stresses $\boldsymbol{\sigma}_{nH}$ appearing in (9) and (10) represent the independent variables of our model which are thus indicated by $\boldsymbol{\sigma}_{nM}$. The equation (9) together with (10) lead to the mixed form of Hooke's law. The weak form of Hooke's law according to the RMVT is:

$$\boldsymbol{\sigma}_{pH} = \mathbf{C}_{pp}\boldsymbol{\epsilon}_{pG} + \mathbf{C}_{pn}\boldsymbol{\sigma}_{nM} \tag{11}$$

$$\boldsymbol{\epsilon}_{nH} = \mathbf{C}_{np}\boldsymbol{\epsilon}_{pG} + \mathbf{C}_{nn}\boldsymbol{\sigma}_{nM} \tag{12}$$

$$\tag{13}$$

where:

$$\begin{aligned}
\mathbf{C}_{pp} &= [\tilde{\mathbf{C}}_{pp} - \tilde{\mathbf{C}}_{pn}(\tilde{\mathbf{C}}_{nn})^{-1}\tilde{\mathbf{C}}_{np}] \\
\mathbf{C}_{pn} &= \tilde{\mathbf{C}}_{pn}(\tilde{\mathbf{C}}_{nn})^{-1} \\
\mathbf{C}_{np} &= -(\tilde{\mathbf{C}}_{nn})^{-1}\tilde{\mathbf{C}}_{np} \\
\mathbf{C}_{nn} &= (\tilde{\mathbf{C}}_{nn})^{-1}
\end{aligned} \tag{14}$$

and $\boldsymbol{\sigma}_{nM}$ are the independent variables of our model.
The geometrical relations can be written in matrix form as:

$$\begin{aligned}
\boldsymbol{\varepsilon}_p &= (\boldsymbol{D}_p + \boldsymbol{A}_p)\boldsymbol{u}\,, \\
\boldsymbol{\varepsilon}_n &= (\boldsymbol{D}_{np} + \boldsymbol{D}_{nz} - \boldsymbol{A}_n)\boldsymbol{u}\,,
\end{aligned} \tag{15}$$

where the differential operators are:

$$\boldsymbol{D}_p = \begin{bmatrix} \frac{\partial_\alpha}{H_\alpha} & 0 & 0 \\ 0 & \frac{\partial_\beta}{H_\beta} & 0 \\ \frac{\partial_\beta}{H_\beta} & \frac{\partial_\alpha}{H_\alpha} & 0 \end{bmatrix}, \quad \boldsymbol{D}_{np} = \begin{bmatrix} 0 & 0 & \frac{\partial_\alpha}{H_\alpha} \\ 0 & 0 & \frac{\partial_\beta}{H_\beta} \\ 0 & 0 & 0 \end{bmatrix}, \quad \boldsymbol{D}_{nz} = \begin{bmatrix} \partial_z & 0 & 0 \\ 0 & \partial_z & 0 \\ 0 & 0 & \partial_z \end{bmatrix}, \tag{16}$$

$$\boldsymbol{A}_p = \begin{bmatrix} 0 & 0 & \frac{1}{H_\alpha R_\alpha} \\ 0 & 0 & \frac{1}{H_\beta R_\beta} \\ 0 & 0 & 0 \end{bmatrix}, \boldsymbol{A}_n = \begin{bmatrix} \frac{1}{H_\alpha R_\alpha} & 0 & 0 \\ 0 & \frac{1}{H_\beta R_\beta} & 0 \\ 0 & 0 & 0 \end{bmatrix}. \tag{17}$$

In RMVT, the compatibility condition of the transverse strains is enforced by equating the second equation of (13) with second equation of (15).

Note that the geometrical relations written for the doubly-curved geometry degenerate in the geometrical relations of plate if radii of curvature R_α and R_β tend to infinite: in this case, the coordinates (α, β, z) can be substituted by (x, y, z).

4. Mixed Interpolated Tensorial Components

According to the finite element method and considering a nine-nodes element, the displacement components and their virtual variations are interpolated on the nodes of the element by means of the classical Lagrangian shape functions N_i:

$$\boldsymbol{u} = N_i \delta \boldsymbol{u}_i \qquad \text{with} \quad i = 1, ..., 9 \tag{18}$$

where $\boldsymbol{u}_i$ are the nodal displacements and their virtual variations.
Considering the local coordinate system (ξ, η) of the element, the MITC shell elements ([37],[38]) are formulated by using, instead of the strain components directly computed from the displacements, an interpolation of these within each element using a specific interpolation strategy for each component. The corresponding interpolation points, called tying points, are shown in figure 7 for a nine-nodes element.
The interpolating functions are calculated by imposing that the function assumes the value 1 in the corresponding tying point and 0 in the others. These are arranged in the following arrays:

$$\begin{aligned}
\bar{N}_1 &= [N_{A1}, N_{B1}, N_{C1}, N_{D1}, N_{E1}, N_{F1}] \\
\bar{N}_2 &= [N_{A2}, N_{B2}, N_{C2}, N_{D2}, N_{E2}, N_{F2}] \\
\bar{N}_3 &= [N_P, N_Q, N_R, N_S]
\end{aligned} \tag{19}$$

Therefore, the in-plane strain components and the shear stresses are interpolated as follows:

$$\varepsilon_{\alpha\alpha} = \bar{N}_{1_m}\varepsilon_{\alpha\alpha_m}\,; \quad \varepsilon_{\beta\beta} = \bar{N}_{2_m}\varepsilon_{\beta\beta_m}\,; \quad \varepsilon_{\alpha\beta} = \bar{N}_{3_m}\varepsilon_{\alpha\beta_m} \tag{20}$$

$$\sigma_{\alpha z} = \bar{N}_{1_m}\sigma_{\alpha z_m} \quad \sigma_{\beta z} = \bar{N}_{2_m}\sigma_{\beta z_m} \tag{21}$$

with $m = 1, \ldots, 6$, except $\varepsilon_{\alpha\beta}$ for which $m = 1, \ldots, 4$. The strain components $\varepsilon_{\alpha\alpha_m}$, $\varepsilon_{\beta\beta_m}$ and $\varepsilon_{\alpha\beta_m}$ still depend on displacements (18) by means of geometrical relations (15) and the shape functions N_i are evaluated in the tying points. From this point on, the subscripts $m1$, $m2$ and $m3$ indicate quantities calculated in the points $(A1, B1, C1, D1, E1, F1)$, $(A2, B2, C2, D2, E2, F2)$ and (P, Q, R, S), respectively. Note that the transverse normal stress σ_{zz} is excluded from this procedure because it doesn't produce locking and it is interpolated on the standard nodes of the element as the displacements:

$$\sigma_{zz} = N_i\sigma_{zz_i} \qquad \text{with} \quad i = 1, \ldots, 9 \tag{22}$$

5. Unified Formulation

The main feature of the Unified Formulation by Carrera [36] (CUF) is the unified manner in which the variables are handled. According to CUF, the displacement field and the transverse stress field are written by means of approximating functions in the thickness direction as follows:

$$\boldsymbol{u}^k(\alpha, \beta, z) = F_\tau(z)\boldsymbol{u}^k_\tau(\alpha, \beta)\,; \quad \boldsymbol{\sigma}^k_n(\alpha, \beta, z) = F_\tau(z)\boldsymbol{\sigma}^k_{n_\tau}(\alpha, \beta) \qquad \tau = 0, 1, ..., N \tag{23}$$

where F_τ are the so-called thickness functions depending only on the coordinate z. $\boldsymbol{u}_\tau$, $\boldsymbol{\sigma}_{n_\tau}$ are the unknown variables depending on the in-plane coordinates α,β and they are approximated by FEM. τ is a sum indexes and N is the order of expansion assumed in the thickness direction (usually $N = 1, ..., 4$).

If one chooses to adopt a Layer-Wise (LW) approach, the variables are defined independently for each layer k of the multilayer as follows:

$$\boldsymbol{u}^k = F_t\,\boldsymbol{u}^k_t + F_b\,\boldsymbol{u}^k_b + F_r\,\boldsymbol{u}^k_r = F_\tau\,\boldsymbol{u}^k_\tau, \qquad \tau = t, b, r\,, \quad r = 2, ..., N. \tag{24}$$

$$\boldsymbol{\sigma}^k_n = F_t\,\boldsymbol{\sigma}^k_{n_t} + F_b\,\boldsymbol{\sigma}^k_{n_b} + F_r\,\boldsymbol{\sigma}^k_{n_r} = F_\tau\,\boldsymbol{\sigma}^k_{n_\tau}, \qquad \tau = t, b, r\,, \quad r = 2, ..., N. \tag{25}$$

$$F_t = \frac{P_0 + P_1}{2}, \quad F_b = \frac{P_0 - P_1}{2}, \quad F_r = P_r - P_{r-2}. \tag{26}$$

in which $P_j = P_j(\zeta_k)$ is the Legendre polynomial of j-order defined in the ζ_k-domain: $-1 \leqslant \zeta_k \leqslant 1$.
In this way, the top (t) and bottom (b) values of are used as unknown variables and one can impose the following compatibility conditions:

$$\boldsymbol{u}^k_t = \boldsymbol{u}^{k+1}_b\,, \quad \boldsymbol{\sigma}^k_{n_t} = \boldsymbol{\sigma}^{k+1}_{n_b}\,, \quad k = 1, N_l - 1 \tag{27}$$

Finally, if one includes the FEM approximation of the previous section, the displacements and transverse stresses can be written as follows:

$$\boldsymbol{u}^k = F_\tau N_i \boldsymbol{u}^k_{\tau i}\,; \quad \boldsymbol{\sigma}^k_n = F_\tau N_i \boldsymbol{\sigma}^k_{n_{\tau i}} \qquad \tau = 0, 1, ..., N \quad \text{and} \quad i = 1, \ldots, 9 \tag{28}$$

where $\boldsymbol{u}^k_{\tau i}$ and $\boldsymbol{\sigma}^k_{n_{\tau i}}$ are the degrees of freedom of the final linear algebraic system.

From this point on, the models here presented will be indicated as LMN (L=layer-wise and M=mixed formulation RMVT) or LDN (L=layer-wise and D=displacement formulation PVD), where N is the order of expansion assumed in the thickness direction.

6. Numerical results

In order to present the performance of our element, we have considered two tests: a laminated plate with [0°/90°/0°] stacking sequence and a cylinder with [90°/0°] stacking sequence.

6.1. Results for $[0°/90°/0°]$ *laminated plate*

A cross-ply laminated plate, with stacking sequence of symmetric $[0°/90°/0°]$, is considered for the analysis. Plate geometric dimensions are $a = 1$ and $b = 3$ (see Fig.7). Plates with different length to thickness (a/h) ratios are considered in simulation, where h is the plate thickness. Plate is loaded with a bisinusoidal transverse pressure, $p_z = \hat{p_z} sin(\frac{\pi x}{a}) sin(\frac{\pi y}{b})$ on the top surface of the plate, with maximum intensity of $\hat{p_z} = 1$. The plate has simply supported boundary conditions. Taking into account the symmetry of the plate in the geometry, boundary conditions and loading, only a quarter of the plate is modelled and meshed for analysis. The plate geometry is meshed with MITC quadrilateral nine-nodes elements. Lamina properties considered in the simulation are: Young's modulus ratio $E_1/E_2 = 25.0$ and $E_2/E_3 = 1.0$, where E_1 is the Young's modulus along the fibre direction, while E_2 and E_3 are the Young's moduli of the material across the fibre direction; Young's modulus to shear modulus ratios of the material are $E_2/G_{12} = 2$, $G_{12}/G_{13} = 1$ and $E_2/G_{23} = 5$; finally, Poisson ratios are $\nu_{12} = \nu_{13} = \nu_{23} = 0.25$.

The presented results are non-dimensional according to the existing 3D elasticity results given in literature [2]. The formulas used are the following:

$$\begin{aligned} \bar{u}_z &= \frac{u_z 100 E_2 h^3}{\hat{p_z} a^4} \\ \bar{\sigma}_{xz} &= \frac{\sigma_{xz}}{\hat{p_z}\left(\frac{a}{h}\right)} \\ \bar{\sigma}_{xx} &= \frac{\sigma_{xx}}{\hat{p_z}\left(\frac{a}{h}\right)^2} \\ \bar{\sigma}_{zz} &= \frac{\sigma_{zz}}{\hat{p_z}\left(\frac{a}{h}\right)} \end{aligned} \tag{29}$$

First of all a convergence study is presented in Table 1. Since MITC9 are supposed to be devoid of shear locking, a plate with $a/h = 100$ is considered. Transverse displacement and stresses with increasing mesh size are calculated by a layer-wise mixed 4th order model (LM4). It is clear from the table that the mesh 5×5 is the most convenient for the following analyses because it ensures a good convergence for both the displacement and the stresses and it requires a lower computational cost.

6.1.1. Locking study

Plate elements having the capability of incorporating shear stiffening effects are prone to shear locking phenomenon. This phenomenon reduces the transverse displacement induced in the structure with decreasing plate thickness, even when the mesh size increases. The following study compares LM4 and LD4 solutions with the solution obtained with LD4 model without applying MITC method, here indicated as $LD4_s$. These results are presented in Table 2 for different thickness ratios a/h, from thick to very thin plates. The transverse displacement is calculated. It can be noted that LM4 model provides almost the same results of LD4 model and both of them differ from the $LD4_s$ solution when the plate is thin $(a/h = 100, 1000)$. This indicates that the shear locking is present, even if it isn't very significant due to the boundary and loading conditions of the plate, and the mixed model LM4, formulated on the basis of MITC interpolation strategy, is able to withstand the locking phenomenon.

6.1.2. Comparision of results for various theories

Comprehensive results obtained using different theories and for plates of different length to thickness ratios are tabulated in Tables 3 and 4. For comparison purposes, also the results computed with classical First-order Shear Deformation Theory (FSDT) are provided. These tables list the results for transversal displacement and the transverse shear stress in x direction. The solution obtained without applying MITC method $LM4_s$ are also tabulated in Table 3: this means that the shear stresses are interpolated using the nodes of the element and the membrane strains are directly computed by geometrical relations. It is seen from the table that for the finite element model $LM4_s$ the results for displacement starts deviating from the reference results for higher length-to-thickness ratios. This fact demonstrates the effectiveness of introducing MITC interpolation in RMVT formulation with respect to the locking phenomenon.

In general, it can be observed that higher-order models are required to correctly predict the 3D solution in terms of transversal displacement for thick plates, while for thin plates all the models, included FSDT, provide similar results. Considering the computation of shear stress, it can be noted that: FSDT model completely fails even when the plate is very thin; LMN and LDN models provide almost the same results for every length-to-thickness ratio and any order of expansion N (as for the transversal displacement).

However, looking at Figure 3 that shows the shear stress distribution through the thickness for plate with length-to-thickness ratio 100, LMN and LDN models present some differences. In particular, the models indicated with suffix $\_M$ provide the shear stress modeled a priori (σ_{xz_M}) while the models $\_H$ provide the shear stress

computed from the displacements by Hooke's law (σ_{xz_H}). The distributions of LMN_M and LDN_M are very similar since the displacements calculated by both the series of models are the same. Also LMN_M models provide similar distributions to the previous ones but only these models are able to satisfy the interlaminar continuity conditions and zero conditions at top and bottom surfaces of the plate. In general, the shear stress profiles from higher order theories are more realistic than those obtained from the lower order theories.

Similar comments can be extended to the transverse normal stress distribution. Normalized normal stress ($\bar{\sigma}_{zz}$) variation across the thickness for different length to thickness ratios of plate are plotted in Figures 4 and 5. Stresses plotted in these figures are obtained using a layer-wise 4-th order mixed model: LM4_M in the first case, LM4_H in the second one. Normal stress σ_{zz} has the following boundary conditions at the location $x = a/2$ and $y = b/2$: unit value at the top surface and zero value at the bottom surface. These boundary conditions are not satisfied by the normal stress obtained using Hooke's law σ_{zz_H}, while they are satisfied by the normal stress $sigma_{zz_M}$ obtained as primary variable in mixed formulation. Finally, it can be seen in Figure 5 that the LM4_H solution completely diverge from the correct profile when the plate is very thin ($a/h = 1000$). This demonstrates again the advantages of using a mixed model.

6.2. Results for cylindrical shells

In order to evaluate the performance of present formulation for layered shell structures, a cylindrical shell with orthotropic laminate stacking sequence [90°/0°] (see Figure 7). A bisinusoidal pressure load $p_z = \hat{p_z} sin(\frac{\pi m \alpha}{L}) sin(\frac{\pi n \beta}{b})$ is applied at the inner surface and the ends of the cylinder are simply supported. Where, $\hat{p_z} = 1$, $m = 1$, $n = 8$, $b = 2\pi R$, R is the curvature radius in β direction and L is the length of the cylinder. The normalized orthotropic material properties considered for the simulation, as in the reference [39], are the same of the previous plate and the layers have equal thickness.

The length of the cylinder considered for simulation is $L = 4R = 40$, where $R = 10$. The number of elements used on an octave of cylinder (half length and a quarter of circumference) is 8×8, that is the convergence mesh. Symmetry boundary conditions are applied at the cut edges. The results are tabulated in non-dimensional form:

$$\begin{aligned} \bar{u}_z &= \frac{u_z 10 E_1 h^3}{\hat{p_z} R^4} \\ \bar{\sigma}_{\alpha\alpha} &= \frac{10 \sigma_{\alpha\alpha}}{\hat{p_z} \left(\frac{R}{h}\right)^2} \\ \bar{\sigma}_{\beta z} &= \frac{10 \sigma_{\beta z}}{\hat{p_z} \left(\frac{R}{h}\right)} \\ \bar{\sigma}_{zz} &= \frac{\sigma_{zz}}{\hat{p_z}} \end{aligned} \tag{30}$$

Table 5 tabulates the displacement normal to the shell reference surface, for different shell geometries. From the table it is evident that for thick shells only the solutions obtained with higher-order models are comparable with the results of the reference article [39]. In particular, it can be noted that in the case of thick shell ($R/h = 2, 4$) the LD4 model is not able to exactly reproduce the reference solution as LM4 model. This behavior is different from the previous study case regarding the plate with symmetric lamination, where LDN and LMN models provided the same results. Since the description of the geometry is the same for both the series of models, this fact can be justified by considering the antisymmetric lamination of the shell: in this case, it is more difficult to describe the transverse stresses, as it will be shown below, and this can have some effects also on the displacements.

6.2.1. Evaluation of stresses

The ability of RMVT formulation for cylindrical shells to capture results accurately is emphasised in the following tables. First of all, Table 6 tabulates the normal stress $\bar{\sigma}_{\alpha\alpha}$ measured at location $(L/2, 90°)$ and bottom and top surfaces of the cylindrical shell by varying the radius-to-thickness ratio. As for the displacements, it is clear that the normal stress obtained using $FSDT$ is off the mark for thick shells, whereas the results obtained using higher order models are comparable to the reference solution, for all radius-to-thickness ratios.

The main advantage of employing mixed formulation is to describe accurately the transverse stresses. For comparison purposes with reference solution, the results for the transverse shear and normal stresses obtained with different theories are tabulated in Tables 7 and 8, by the varying the radius-to-thickness ratio. FSDT theory is not capable of capturing the transverse shear stress even when the shell is very thin (transverse normal stress is assumed zero). Only the transverse stress results from the higher-order model are comparable with the reference solution, even when thin shells are studied. This can be explained looking at the distributions of transverse shear stress in Figures 9 ($R/h = 4$) and 10 ($R/h = 500$) and transverse normal stress in Figures 7 ($R/h = 4$) and 8 ($R/h = 500$). Here, lower order mixed models (LM2) are compared with higher order mixed models (LM4) and the stresses are

both modeled a priori (M) and derived from the displacements (H). It can be noted that LMN_H models provide always distributions that are different from LMN_M results: in particular, the interlaminar continuity conditions or top/bottom homogeneous conditions are not satisfied. Moreover, it is shown that mixed models M with lower order of expansion are not able to describe correctly the transverse stresses profile in the thick shell, although the continuity conditions are fulfilled. In the case of transverse normal stress, this happens even when the shell is very thin. It can be concluded that in multilayered structures, especially antisymmetric ones, the transverse stresses should be evaluated a priori by using higher-order models in order to be correctly predicted.

7. Conclusions

In this work, some advanced shell models based on Reissner Mixed Variational Theorem are presented and compared with shell models based Principle of Virtual Displacements in the analysis of multilayered orthotropic structures. A strategy similar to MITC (Mixed Interpolated of Tensorial Components) approach is introduced for the interpolation of transverse shear stresses in order to have a locking-free finite element. Moreover, assuming the transverse stresses as independent variables, the continuity at the interfaces between layers has been directly imposed. A plate with symmetric lamination and a cylindrical shell with antisymmetric lamination have been analyzed.
It has been demonstrated that in the MITC context, the element exhibits both properties of convergence and robustness when comparing the numerical results with benchmark solutions from literature, and the formulation is devoid of shear locking even for higher span to thickness ratios.
By comparing the different models and considering various span-to-thickness ratios, it can be concluded that:

- higher-order models are required for the analysis of thick structures;
- models based on PVD don't always satisfy interlaminar continuity conditions (and homogeneous conditions);
- the results of models based on PVD differ mostly from the RMVT results when the lamination is antisymmetric;
- in a mixed formulation, if the transverse stresses are computed by the Hooke's law the results are the same of models based on displacement formulation.

Finally, it has been demonstrated that a correct description of transverse stresses requires necessarily the use of higher-order mixed models and this fact is independent from the span-to-thickness ratio: the risk is to get a through-the-thickness distribution completely different from the reality.

Acknowledgement

The second author Keshava Kumar S. would like to thank Erasmus Mundus Heritage fellowship for providing the scholarship under PhD mobility to conduct this research work at Politecnico di Tornio. He would also like to thank Prof. Dineshkumar Harursampath for supporting his candidature for the Erasmus fellowship and timely suggestions during the mobility.
E. Carrera acknowledges the Russian Science Foundation under grant N 18-19-00092.

Data Availability

The raw/processed data required to reproduce these findings cannot be shared at this time due to technical or time limitations.

References

[1] J. Whitney, The Effect of Transverse Shear Deformation on the Bending of Laminated Plates, Journal of Composite Materials 3 (3) (1969) 534–547.

[2] N. Pagano, Exact Solutions for Composite Laminates in Cylindrical Bending, Journal of Composite Materials 3 (3) (1969) 398–411.

[3] M. Cinefra, C. Chinosi, L. D. Croce, E. Carrera, Refined shell finite elements based on RMVT and MITC for the analysis of laminated structures, Composite Structures 113 (2014) 492 – 497.

[4] E. Reissner, On a certain mixed variational theorem and a proposed application, International Journal for Numerical Methods in Engineering 20 (7) (1984) 1366–1368.

[5] E. Reissner, On a mixed variational theorem and on shear deformable plate theory, International Journal for Numerical Methods in Engineering 23 (2) (1986) 193–198.

[6] E. Reissner, On a certain mixed variational theorem and on a laminated elastic shell theory, in: Proceedings of Euromech-Colloquium, vol. 219, Proceedings of Euromech-Colloquium, 17–27, 1986.

[7] E. Carrera, Developments, ideas, and evaluations based upon Reissner's Mixed Variational Theorem in the modeling of multilayered plates and shells, Applied Mechanics Review 54 (4) (2001) 301–329.

[8] H. Murakami, Laminated composite plate theory with improved in-plane responses, in: ASME Proc. of PVP Conf., New Orleans, vol. 98-2, ASME Proc. of PVP Conf., New Orleans, 257–263, 1985.

[9] H. Murakami, Laminated composite plate theory with improved in-plane responses, Journal of Applied Mechanics 53 (1986) 661–666.

[10] A. Toledano, H. Murakami, A high-order laminated plate theory with improved in-plane responses, International Journal of Solids and Structures 23 (1) (1987) 111 – 131.

[11] A. Toledano, H. Murakami, A composite plate theory for arbitrary laminate configurations,, Journal of Applied Mechanics 54 (1987) 181–189.

[12] K. Soldatos, Cylindrical bending of cross-ply laminated plates: refined 2D plate theories in comparison with the exact 3D elasticity solution, Tech. Rep. 140, Dept. of Math., University of Ioannina, Greece, 1987.

[13] E. Carrera, A class of two-dimensional theories for anisotropic multilayered plates analysis, in: Accademia delle Scienze di Torino, Memorie Scienze Fisiche, 19–20, Accademia delle Scienze di Torino, Memorie Scienze Fisiche, 11–39, 1995.

[14] E. Carrera, CZ0 Requirements–models for the two dimensional analysis of multilayered structures, Composite Structures 37 (3) (1997) 373 – 383.

[15] E. Carrera, A Reissner's mixed variational theorem applied to vibration analysis of multilayered shells, Journal of Applied Mechanics 66 (1999) 69–78.

[16] E. Carrera, Mixed layer-wise models for multilayered plates analysis, Composite Structures 43 (1) (1998) 57 – 70.

[17] E. Carrera, Evaluation of layer-wise mixed theories for laminated plates analysis, AIAA Journal 36 (5) (1998) 830–839.

[18] E. Carrera, Transverse normal stress effects in multilayered plates, Journal of Applied Mechanics 66 (4) (1999) 1004–1012.

[19] E. Carrera, A Study of Transverse Normal Stress Effect on Vibration of Multilayered Plates and Shells, Journal of Sound and Vibration 225 (5) (1999) 803 – 829.

[20] E. Carrera, Single-layer vs multi-layers plate modelings on the basis of Reissner's mixed theorem, AIAA Journal 38 (2) (2000) 342–352.

[21] E. Carrera, A priori vs. a posteriori evaluation of transverse stresses in multilayered orthotropic plates, Composite Structures 48 (4) (2000) 245 – 260.

[22] E. Carrera, Vibrations of layered plates and shells via Reissner's Mixed Variational Theorem, in: Fourth Symposiom on Vibrations of Continuos Systems, Kenswick, 4–6, 2003.

[23] E. Carrera, Layer-wise mixed models for accurate vibration analysis of multilayered plates, ASME Journal of Applied Mechanics 65 (1998) 820–828.

[24] A. Messina, Two Generalized Higher Order Theories in Free Vibration Studies of Multilayered Plates, Journal of Sound and Vibration 242 (1) (2001) 125 – 150.

[25] E. Carrera, L. Demasi, Sandwich plates analyses by finite element method and Reissner's Mixed Theorem, in: Sandwich V, 301–313, 2000.

[26] E. Carrera, L. Demasi, Classical and advanced multilayered plate elements based upon PVD and RMVT. Part 1: Derivation of finite element matrices, International Journal for Numerical Methods in Engineering 55 (2) (2002) 191–231.

[27] E. Carrera, L. Demasi, Classical and advanced multilayered plate elements based upon PVD and RMVT. Part 2: Numerical implementations, International Journal for Numerical Methods in Engineering 55 (3) (2002) 253–291.

[28] O. C. Zienkiewicz, R. L. Taylor, J. M. Too, Reduced integration technique in general analysis of plates and shells, International Journal for Numerical Methods in Engineering 3 (2) (1971) 275–290.

[29] H. Hou-Cheng, Membrane locking and assumed strain shell elements, Computers & Structures 27 (5) (1987) 671 – 677.

[30] F. Brezzi, K.-J. Bathe, M. Fortin, Mixed-interpolated elements for Reissner–Mindlin plates, International Journal for Numerical Methods in Engineering 28 (8) (1989) 1787–1801.

[31] C. Chinosi, L. Della Croce, Mixed-interpolated elements for thin shells, Communications in Numerical Methods in Engineering 14 (12) (1998) 1155–1170.

[32] K.-J. Bathe, P.-S. Lee, J.-F. Hiller, Towards improving the MITC9 shell element, Computers & Structures 81 (8) (2003) 477 – 489.

[33] P. Panasz, K. Wisniewski, Nine-node shell elements with 6 dofs/node based on two-level approximations. Part I, Finite Elements in Analysis and Design 44 (12) (2008) 784 – 796.

[34] M. Cinefra, C. Chinosi, L. D. Croce, MITC9 Shell Elements Based on Refined Theories for the Analysis of Isotropic Cylindrical Structures, Mechanics of Advanced Materials and Structures 20 (2) (2013) 91–100.

[35] M. Cinefra, E. Carrera, Shell finite elements with different through-the-thickness kinematics for the linear analysis of cylindrical multilayered structures, International Journal for Numerical Methods in Engineering 93 (2) (2013) 160–182.

[36] E. Carrera, Theories and finite elements for multilayered, anisotropic, composite plates and shells, Archives of Computational Methods in Engineering 9 (2) (2002) 87–140.

[37] K.-J. Bathe, E. N. Dvorkin, A formulation of general shell elements—the use of mixed interpolation of tensorial components, International Journal for Numerical Methods in Engineering 22 (3) (1986) 697–722.

[38] M. L. Bucalem, K. J. Bathe, Higher-order MITC general shell elements., Int. J. Numer. Meth. Engng. 36 (1993) 3729–3754.

[39] T. Varadan, K. Bhaskar, Bending of laminated orthotropic cylindrical shells—An elasticity approach, Composite Structures 17 (2) (1991) 141 – 156.

Mesh	$\bar{u}_z(a/2,b/2,0)$	$\bar{\sigma}_{xz}(0,b/2,0)$	$\bar{\sigma}_{xx}(a/2,b/2,h/2)$	$\bar{\sigma}_{zz}(a/2,b/2,0)$
2×2	0.5079	-0.4610	0.6542	0.5023
4×4	0.5076	-0.4449	0.6322	0.5002
5×5	0.5076	-0.4429	0.6294	0.5000
6×6	0.5076	-0.4418	0.6279	0.5000
8×8	0.5076	-0.4407	0.6263	0.5000
10×10	0.5076	-0.4402	0.6256	0.5000
3D[2]	0.508	0.439	0.624	

Table 1: Convergence check for $\bar{u}_z$, $\bar{\sigma}_{xz}$, $\bar{\sigma}_{xx}$ and $\bar{\sigma}_{zz}$ considering LM4 theory and $a/h = 100$.

	$\bar{u}_z(a/2,b/2,0)$		
	$a/h = 10$	$a/h = 100$	$a/h = 1000$
3D[2]	0.919	0.508	–
LM4	0.9189	0.5076	0.5034
LD4	0.9189	0.5076	0.5034
$LD4_s$	0.9189	0.5075	0.5020

Table 2: Shear locking study for the laminated plate [0°/90°/0°].

a/h	$\bar{u}_z(a/2,b/2,0)$				
	4	10	20	100	1000
3D[2]	2.820	0.919	0.610	0.508	
LM4	2.8212	0.9189	0.6095	0.5076	0.5034
$LM4_s$	2.8210	0.9187	0.6093	0.5066	0.5005
LM3	2.8210	0.9189	0.6096	0.5077	0.5034
LM2	2.8103	0.9186	0.6095	0.5077	0.5034
LM1	2.7295	0.9096	0.6077	0.5076	0.5034
LD4	2.8211	0.9189	0.6095	0.5076	0.5034
LD3	2.8210	0.9189	0.6095	0.5076	0.5034
LD2	2.7983	0.9181	0.6094	0.5077	0.5034
LD1	2.7209	0.8989	0.6040	0.5072	0.5032
FSDT	2.0547	0.75315	0.5659	0.50588	0.5034

Table 3: Comparison of different theories to evaluate transverse displacement $\bar{u}_z(a/2,b/2,0)$.

a/h	$\bar{\sigma}_{xz}(0,b/2,0)$				
	4	10	20	100	1000
3D[23]	0.387	0.420	0.434	0.439	
LM4	-0.3544	-0.4236	-0.4380	-0.4429	-0.4431
LM3	-0.3539	-0.4236	-0.4380	-0.4429	-0.4431
LM2	-0.3286	-0.4114	-0.4285	-0.4343	-0.4346
LM1	-0.3499	-0.4207	-0.4364	-0.4420	-0.4422
LD4	-0.3539	-0.4236	-0.4379	-0.4429	-0.4431
LD3	-0.3539	-0.4235	-0.4379	-0.4429	-0.4431
LD2	-0.3500	-0.4226	-0.4371	-0.4421	-0.4423
LD1	-0.3554	-0.4238	-0.4374	-0.4420	-0.4422
FSDT	-0.1581	-0.1592	-0.1593	-0.1594	-0.1594

Table 4: Comparison of different theories to evaluate the transverse shear stress $\bar{\sigma}_{xz}(0,b/2,0)$.

R/h	2	4	50	500
$\bar{\sigma}_{\beta z}(z = h/4)$[39]	-2.931	-4.440	-4.785	-0.227
LM4	-3.0914	-4.6672	-5.0185	-0.2443
LM3	-3.1813	-4.7217	-5.0191	-0.2443
LM2	-2.8692	-4.3097	-4.5725	-0.2232
LM1	-2.3536	-3.4266	-3.5817	-0.1767
LD4	-3.216	-4.791	-5.024	-0.2441
FSDT	-2.664	-3.216	-2.065	0.3343

Table 7: $\bar{\sigma}_{\beta z}$ measured at $(L/2, 22.5°)$.

R/h	2	4	50	500
$\bar{u}_z(z = 0)$[39]	14.034	6.100	2.242	0.1005
LM4	14.0329	6.0993	2.2422	0.1007
LM3	14.0787	6.1032	2.2422	0.1007
LM2	13.6028	6.0014	2.2417	0.1007
LM1	13.0120	5.9991	2.2431	0.1007
LD4	14.33	6.164	2.242	0.1007
FSDT	12.41	5.578	2.240	0.1007

Table 5: Deflection normal to shell reference surface measured at $(L/2, 90°)$.

R/h	2	4	50	500
$\bar{\sigma}_{\alpha\alpha}(z = \mp h/2)$[39]	-2.660	-0.9610	1.610	0.9436
	0.2511	0.2120	0.2189	0.0449
LM4	-2.7051	-0.9826	1.6038	0.9484
	0.2483	0.2150	0.2237	0.0453
LM3	-2.721	-0.9817	1.6038	0.9484
	0.2474	0.2211	0.2238	0.0453
LM2	-2.6555	-0.9854	1.6023	0.9484
	0.2053	0.1863	0.2207	0.0453
LM1	-2.0171	-0.9550	1.5837	0.9475
	0.0406	0.1094	0.2389	0.04629
LD4	-2.678	-0.9557	1.606	0.9484
	0.2578	0.2210	0.2241	0.04536
FSDT	-1.216	-0.6911	1.603	0.9484
	0.2256	0.2018	0.2216	0.04535

Table 6: Normal stress $\bar{\sigma}_{\alpha\alpha}$ measured at $(L/2, 90°)$.

R/h	2	4	50	500
$\bar{\sigma}_{zz}(z = h/4)$[39]	-0.31	-0.70	-6.29	-3.09
LM4	-0.3167	-0.7078	-6.5436	-3.1999
LM3	-0.3190	-0.7110	-6.5440	-3.1999
LM2	-0.3071	-0.6611	-5.5849	-2.7514
LM1	-0.3261	-0.6659	-4.854	-2.3832
LD4	-0.3408	-0.7358	-6.549	-3.082
FSDT	-	-	-	-

Table 8: $\bar{\sigma}_{zz}$ measured at $(L/2, 90°)$.

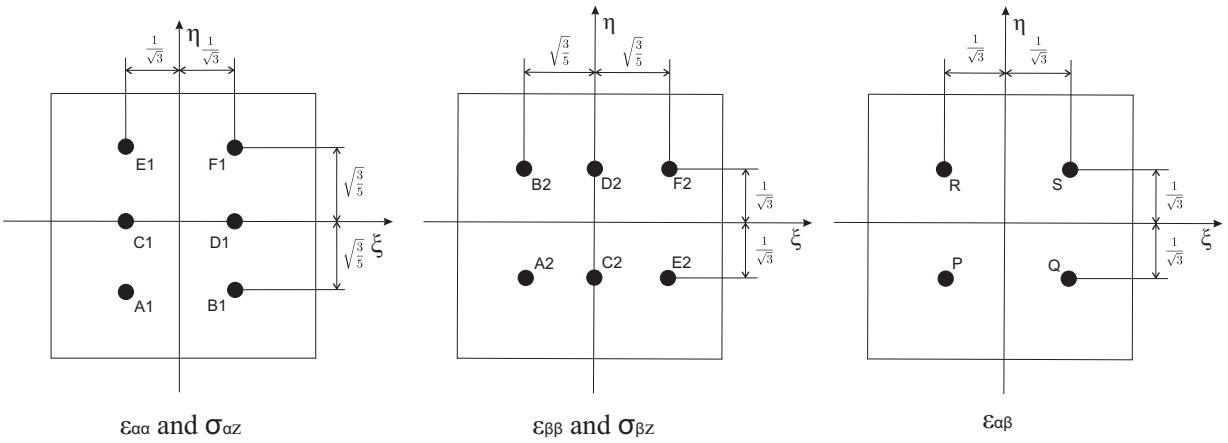

Figure 1: Tying points for the MITC9 shell finite elements.

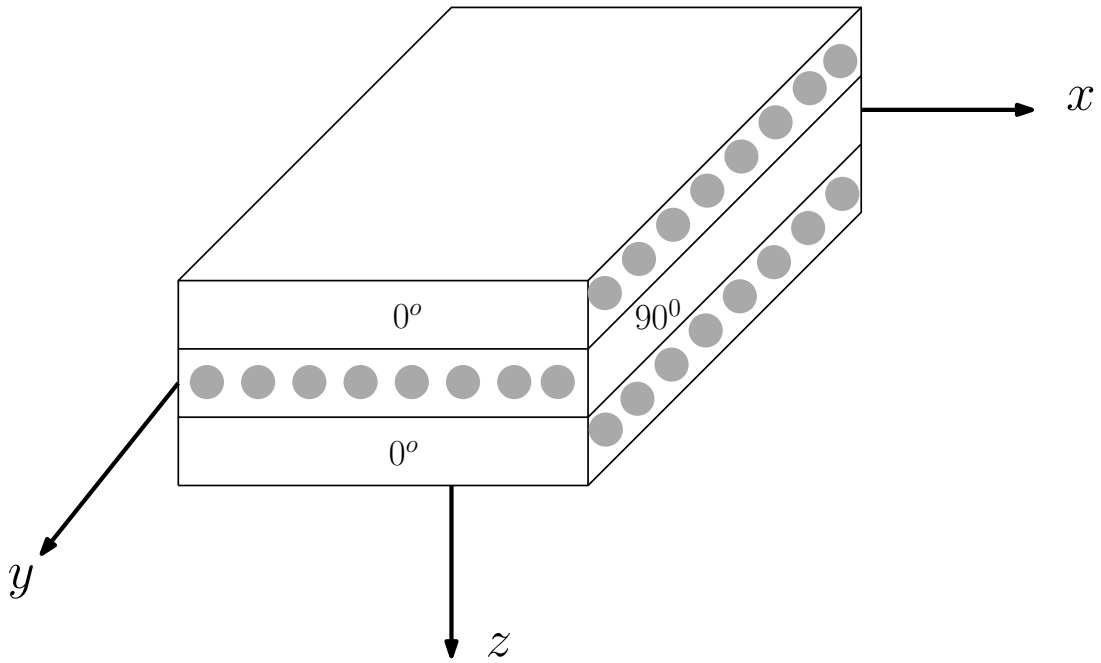

Figure 2: Laminated plate with stacking sequence [0°/90°/0°].

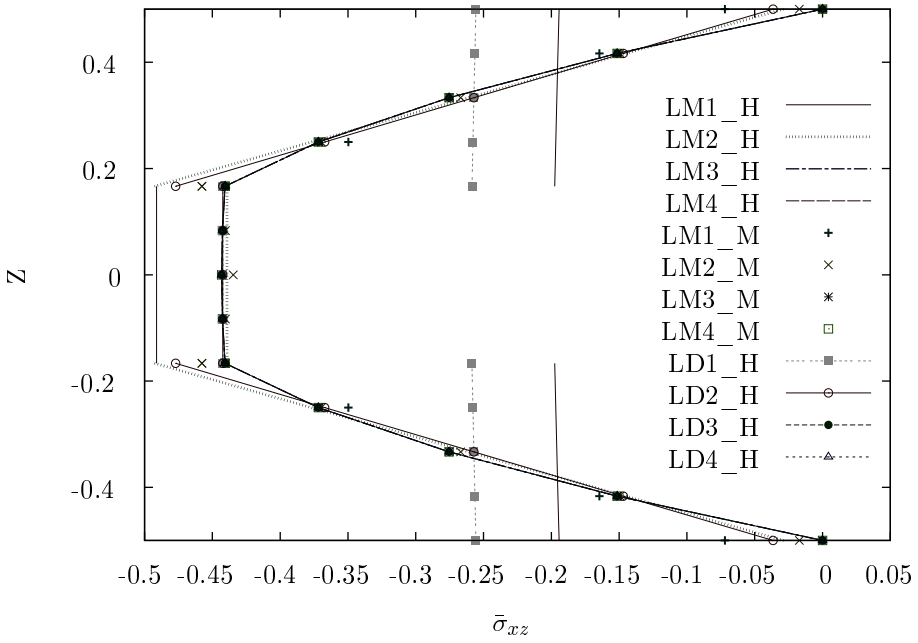

Figure 3: $\bar{\sigma}_{xz}(0, b/2)$ comparison for apriori and posteriori calculations for a/h=100.

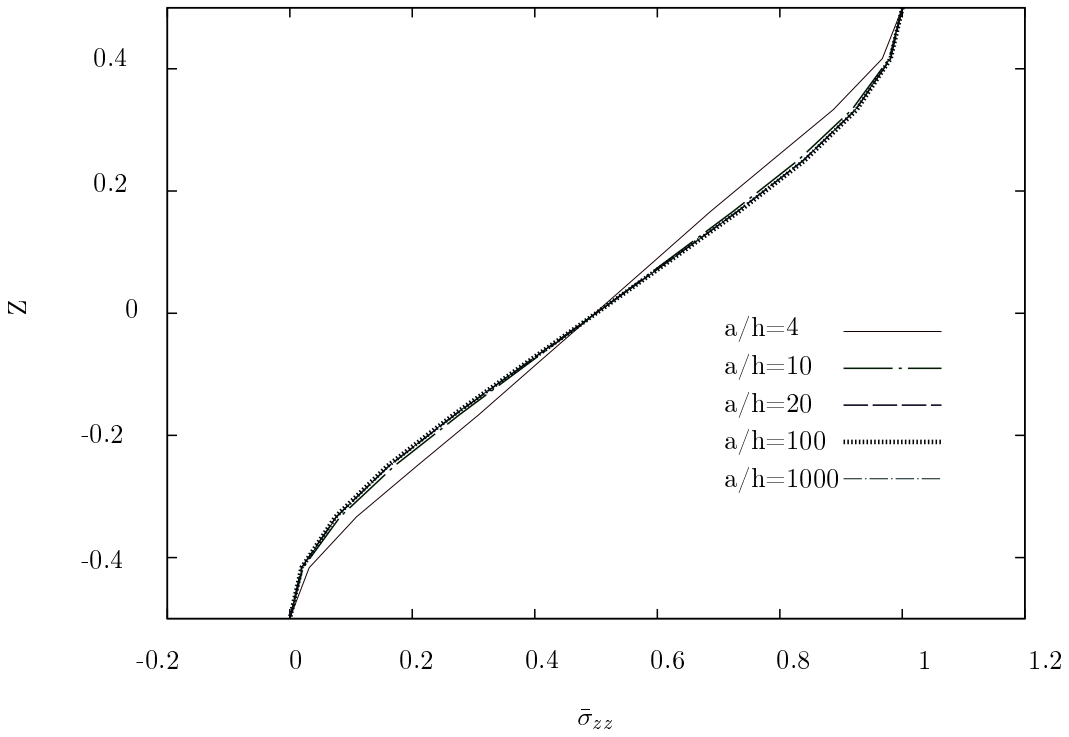

Figure 4: $\bar{\sigma}_{zz}(a/2, b/2)$ (mixed formulation) distribution for different span to thickness ratio.

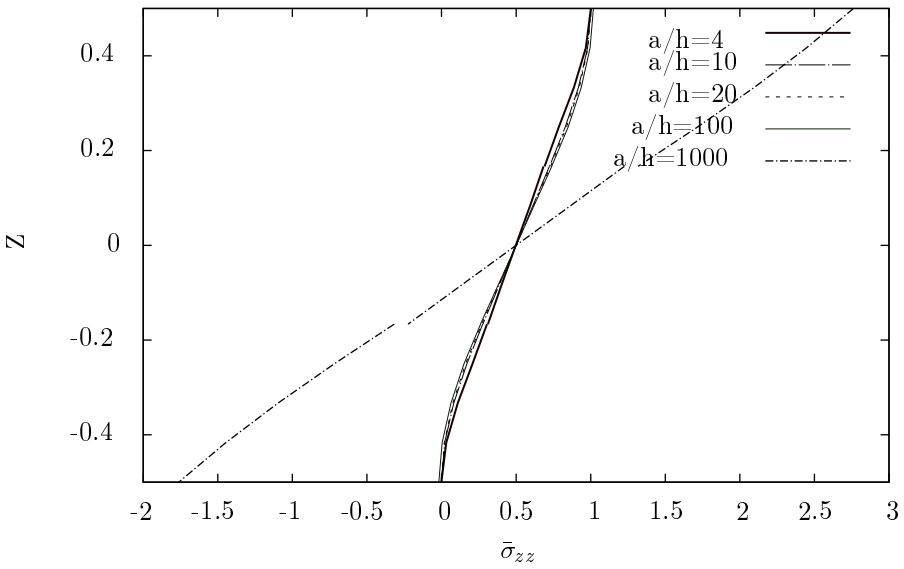

Figure 5: $\bar{\sigma}_{zz}(a/2, b/2)$ (displacement formulation) distribution for different span to thickness ratio.

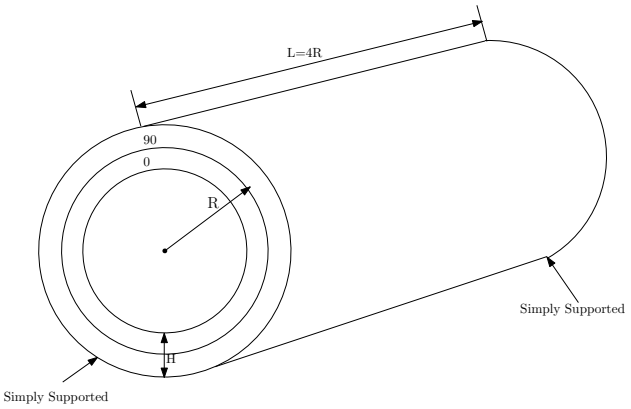

Figure 6: Laminated cylinder with stacking sequence [90°/0°].

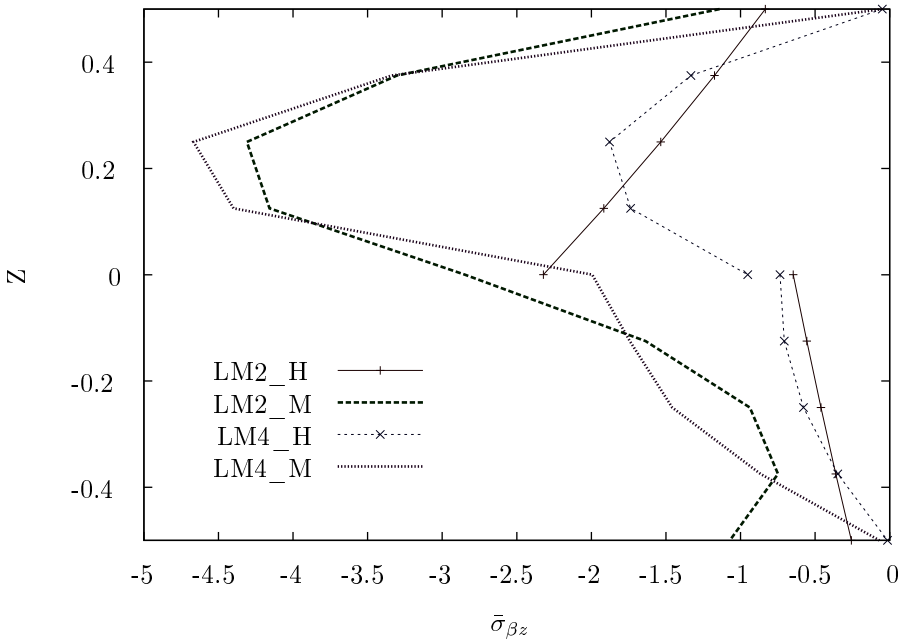

Figure 7: $\bar{\sigma}_{\beta z}(L/2, 67.5^o)$ plot comparison for $R/h = 4$.

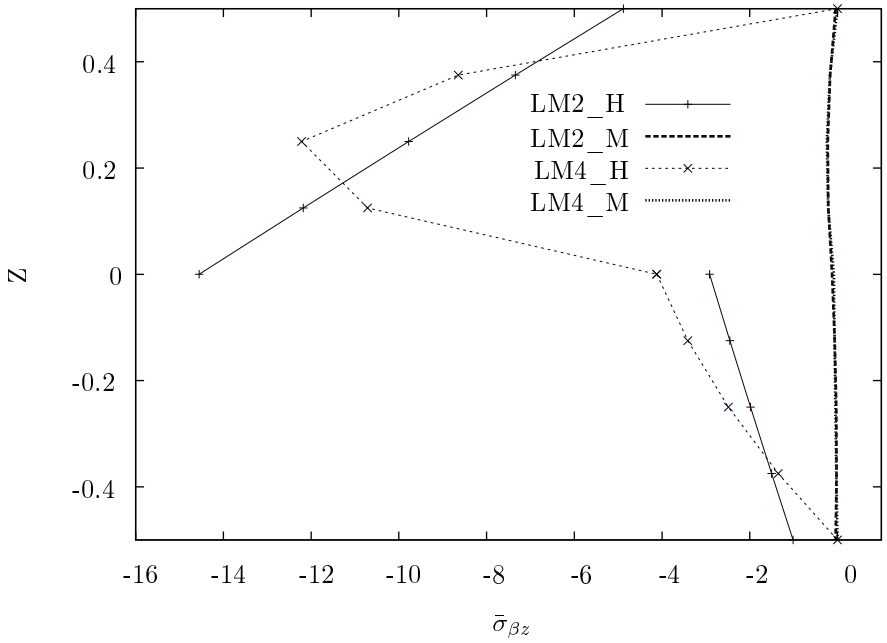

Figure 8: $\bar{\sigma}_{\beta z}(L/2, 67.5^o)$ plot comparison for $R/h = 500$.

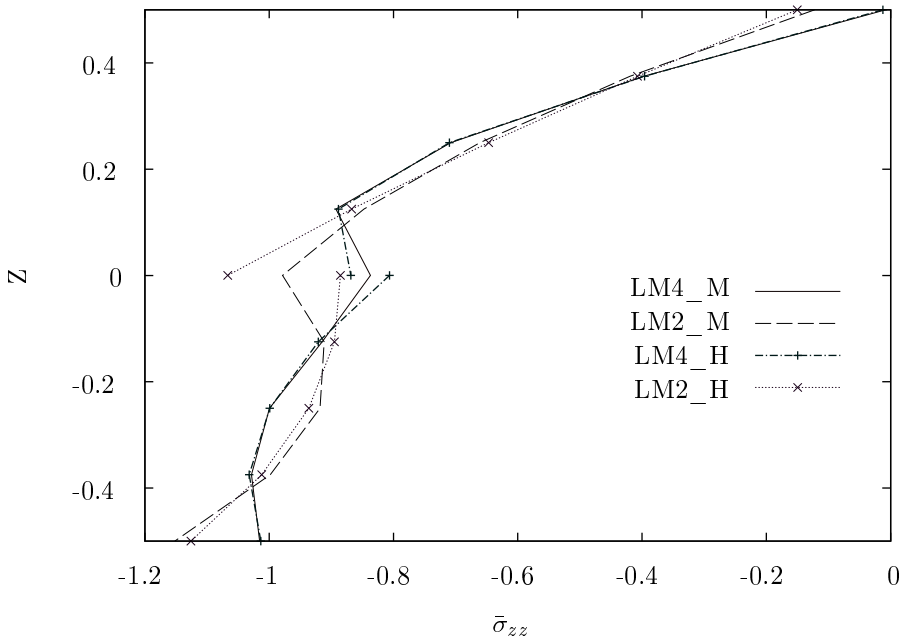

Figure 9: $\bar{\sigma}_{zz}(L/2, 90^o)$ plot comparison for $R/h = 4$.

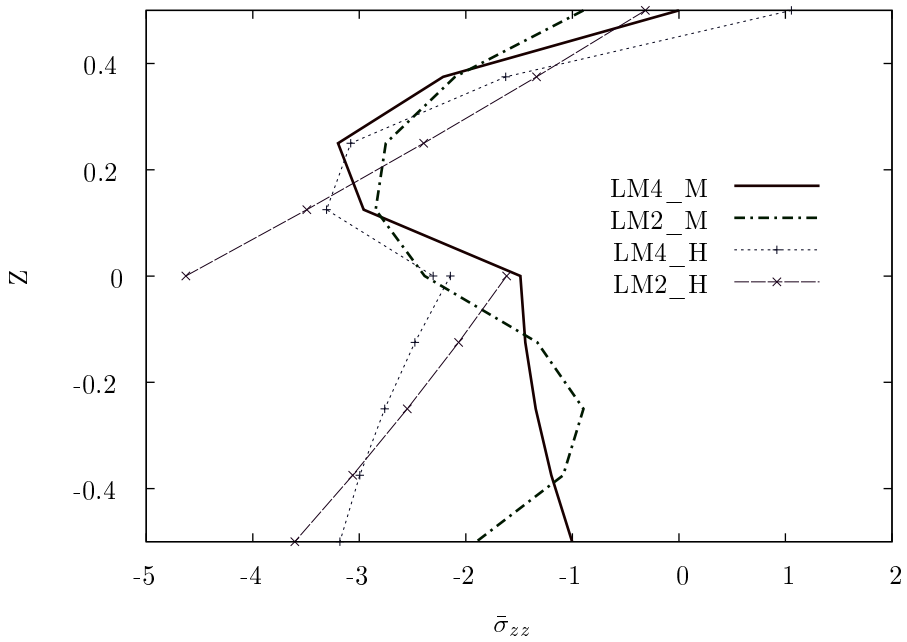

Figure 10: $\bar{\sigma}_{zz}(L/2, 90^o)$ plot comparison for $R/h = 500$.